

A Resonantly-Excited Disk-Oscillation Model of High-Frequency QPOs of Microquasars

Shoji KATO

2-2-2 Shikanoda-Nishi, Ikoma-shi, Nara, 630-0114

kato@gmail.com, kato@kustastro.kyoto-u.ac.jp

(Received 2012 0; accepted 2012 0)

Abstract

A possible model of twin high-frequency QPOs (HF QPOs) of microquasars is examined. The disk is assumed to have global magnetic fields and to be deformed with a two-armed pattern. In this deformed disk, set of a two-armed ($m = 2$) vertical p-mode oscillation and an axisymmetric ($m = 0$) g-mode oscillation are considered. They resonantly interact through the disk deformation when their frequencies are the same. This resonant interaction amplifies the set of the above oscillations in the case where these two oscillations have wave energies of opposite signs. These oscillations are assumed to be excited most efficiently in the case where the radial group velocities of these two waves vanish at the same place. The above set of oscillations is not unique, depending on the node number, n , of oscillations in the vertical direction. We consider that the basic two sets of oscillations correspond to the twin QPOs. The frequencies of these oscillations depend on disk parameters such as strength of magnetic fields. For observational mass ranges of GRS 1915+105, GRO J1655-40, XTE J1550-564, and H1743-322, spins of these sources are estimated. High spins of these sources can be described if the disks have weak poloidal magnetic fields as well as toroidal magnetic fields of moderate strength. In this model the 3 : 2 frequency ratio of high-frequency QPOs is not related to their excitation, but occurs by chance.

Key words: accretion, accretion disks — black holes — quasi-periodic oscillations — X-rays; stars

1. Introduction

Many quasi-periodic oscillations (QPOs) have been observed in low-mass X-ray binaries (LMXBs). Among them, high frequency QPOs are particularly interesting, since they will be attributed to the innermost regions of relativistic accretion disks and thus clarification of their origins will give important informations about disk structure in strong gravitational fields

as well as about mass and spin of the central sources. High frequency QPOs in LMXBs are classified into two classes: High frequency QPOs (HF QPOs) in black-hole LMXBs and kHz QPOs in neutron-star LMXBs (van der Klis 2004). HF QPOs of black-hole LMXBs have no time variation and in some sources they are observed in pairs whose frequency ratio is close to $3 : 2$. kHz QPOs in neutron-star LMXBs are also observed in some sources in pairs, but their frequency ratio is not $3 : 2$, but changes with correlated time variations. It is unclear whether both types of QPOs come from a common origin.

So far, many models have been proposed to describe HF QPOs of black-hole LMXBs, especially focusing on the $3 : 2$ frequency ratio. Typical models will be the relativistic precession model proposed in a series of papers by Stella & Vietri (1998) and Morisink & Stella (1999), and the epicyclic resonant model proposed by Kluźniak & Abramowicz (2001) and Abramowicz & Kluźniak (2001) and extensively studied by their collaborators (e.g., Abramowicz et al. 2003a, b; Bursa et al. 2004; Rebusco 2004, Kluźniak et al. 2004, Horák 2008, Stuchlik et al. 2008a, b, Horák et al 2009 and others). In a context different from the epicyclic resonant model, importance of a resonance on wave excitation has been emphasized, and the warp resonant model has been proposed (Kato 2003, 2004, 2008, Kato & Fukue 2006, Ferreira & Ogilvie 2008, Ohtariani et al. 2010). This model is based on resonant excitation of a set of positive-energy and negative-energy oscillations by interaction through disk deformation (Kato et al. 2011, Kato 2011b). In addition to the above models, many discoseismic modes have been studied in order to examine their applicability to QPOs since Kato & Fukue (1980) (see Wagoner 1999, Kato 2001 and Kato et al. 2008 for reviews, and Wagoner 2012 for recent work).

In spite of many efforts by the above-mentioned work and by other reseraches, the twin QPOs observed in microquasars are not consistently described by one unique model (Török et al. 2011). This difficulty becomes prominent by recent findings that microquasars with twin QPOs have extremely high spins (McClintock et al. 2011).

In the case of kHz QPOs in neutron-star LMXBs, frequencies of twin QPOs and their time variation seem to be well described by assuming that kHz QPOs are two-armed vertical p-mode oscillations trapped in the innermost region of disks (Kato 2011a,c,; 2012a,b,c). In the case of twin HF QPOs of black-hole LMXBs, however, a direct application of trapped vertical p-mode oscillations seems not to well describe observations.

One of important clues to explore the origins of the twin HF QPOs of black-hole LMXBs will be why they appear only in or near to the very high state (steep power-law state) (Remillard 2005), where the disk consists of both a power-law component and a thermal disk component. In the present paper we assume that in the very high state the innermost disk is deformed from an axisymmetric one to a two-armed one,¹ although the origin of the deformation is not

¹ In the warp resonant model (Kato 2004, 2008; Kato & Fukue 2006) the disk deformation was assumed to be one-armed.

explored.² In such deformed disks we impose a set of a two-armed ($m = 2$) vertical p-mode oscillation with negative energy and an axisymmetric ($m = 0$) g-mode oscillation with positive energy. They have the same frequency. We then examine in what cases the set of the oscillations are resonantly excited through the disk deformation in order to apply the results to the HF QPOs in black-hole LMXBs.

As is shown below, we consider two sets of the oscillations. The frequency ratio of these two set of oscillations derived by the present model is not always $3 : 2$, depending on disk parameters. In the present model, magnetic fields in disks are important parameters to specify the frequencies of resonantly interacting oscillations. By adjusting the parameters in reasonable ranges, we examine whether we can describe the frequencies of twin HF QPOs of high-spin microquasars (GRS 1915+105, GRO J1655-40, XTE J1550-564, and H1743-322). One of important parameters is strength of poloidal magnetic fields, because the radial epicyclic oscillations are strongly modified by poloidal magnetic fields (Fu & Lai 2009).

2. Outline of Present Model of HF twin QPOs

2.1. Two-Armed-Deformed Disks

As mentioned above, we assume that in the transition to the very high state the disk is deformed to a state with a two-armed pattern. The pattern may rotate slowly in the azimuthal direction with frequency ω_D . In this paper, for simplicity, the pattern is assumed just standing, $\omega_D = 0$. (A generalization to a case of $\omega_D \neq 0$ is simple.) We further assume that the two-armed deformation consists of two components concerning the node number(s) in the vertical direction. One is the deformation with one node in the vertical direction, i.e., $n_D = 1$, and the other with $n_D = 2$. A $n_D = 1$ deformation is the lowest mode of deformations which is asymmetric with respect to the equator. In summary, the sets of frequency, ω_D , azimuthal wavenumber m_D , and the vertical node number n_D of the deformation, (ω_D, m_D, n_D) , are both $(0, 2, 1)$ and $(0, 2, 2)$.

2.2. Two Types of Oscillations and Their Propagation Regions

Let us consider a set of oscillations. One is an axisymmetric ($m = 0$) g-mode oscillation, and the other is a two-armed ($m = 2$) vertical p-mode oscillation (see, e.g., Kato 2001 and Kato et al. 2008 for classification of disk oscillations). They are assumed to have the same frequency. These two oscillations can resonantly interact each other through the two-armed disk deformation, since the difference between the azimuthal wavenumbers is two and equal to m_D .³ This resonant interaction through the disk deformation can excite these two oscillations

² There are numerical simulations showing a deformation of the innermost part of disks. Machida & Matsumoto (2008) show that in a cool state of magnetized accretion disks, a torus is created in the innermost part of disks and deformed into a crescent-like shape.

³ For the resonant interaction to occur, in addition to this condition concerning the difference of azimuthal wavenumbers, the difference of the vertical node numbers of the two oscillations must be 1 or 2. This is

simultaneously when wave energies of these oscillations have opposite signs (Kato et al. 2011, Kato 2011b, see also Kato 2008).

The axisymmetric g-mode oscillation has a positive energy because of the very fact of axisymmetry. The two-armed vertical p-mode oscillation has two propagation regions in the radial direction; inner and outer propagation regions. Between them, there are evanescent region and the radius of corotation resonance. It is generally known that in the inner propagation region waves has a negative energy, while those in the outer propagation region have a positive energy (e.g., Kato 2001).⁴ Hence, if the propagation region of the axisymmetric g-mode oscillation and the inner propagation region of the two-armed vertical p-mode oscillation are spatially overlapped, we can expect simultaneous growth of these two oscillations with the same frequency by their resonant coupling through the disk deformation. The spatial overlapping of propagation region really occurs, as is shown below and in figures 1 and 2.

Before discussing one more resonant condition which we adopt in this paper, we must notice the propagation regions of the two-armed vertical p-mode oscillation and of the axisymmetric g-mode oscillation, and their parameter dependences. First, we consider the m -armed vertical p-mode oscillations. At the boundary between the propagation and evanescent regions, the oscillations have long wavelength in the radial direction, and the relation between the frequency and boundary radius can be obtained by considering purely vertical oscillations (e.g., Kato 2011a). In the case of vertically isothermal disks with no magnetic fields, by solving the vertical eigen-value problem for purely vertical oscillations we find that the relation is given by

$$(\omega - m\Omega)^2 = n\Omega_{\perp}^2 \quad (1)$$

(cf., Okazaki et al. 1987), where $\Omega(r)$ is the angular velocity of disk rotation at the radius r , $\Omega_{\perp}(r)$ is the vertical epicyclic frequency, and n is a positive integer specifying the number of node of oscillations in the vertical direction, i.e., $n = 1, 2, \dots$ ⁵

In the case of adiabatic oscillations in polytropic gases with polytropic index N , the radii where the vertical p-mode oscillations become purely vertical are

$$(\omega - m\Omega)^2 = \begin{cases} \Omega_{\perp}^2 & (n = 1) \\ (1 + \gamma)\Omega_{\perp}^2 & (n = 2) \\ 3\gamma\Omega_{\perp}^2 & (n = 3) \end{cases} \quad (2)$$

(Perez et al. 1997, Silbergleit et al. 2001, Kato 2005), where $\gamma = 1 + 1/N$. If the disk are

related to the fact that n_{D} is taken to $n_{\text{D}} = 1$ and $n_{\text{D}} = 2$. As will be discussed later, we consider axisymmetric g-mode oscillations with $n = 1$ and two-armed vertical p-mode oscillations with $n = 2$ and $n = 3$. Hence, this condition is satisfied.

⁴ Let us consider an oscillation whose frequency is ω and the azimuthal wavenumber is m . Then, the corotation resonance occurs at the radius where $\omega = m\Omega$. One of the propagaion region of the oscillation is inside the corotation radius, and the oscillation in the region has a negative energy since $\omega - m\Omega < 0$ there.

⁵ In the case of vertical p-mode oscillations, n starts from 1. The case of $n = 0$ is the p-mode.

vertically isothermal but terminated at a certain height, z_s , by hot corona, and subject to toroidal magnetic fields which are distributed in the vertical direction so that c_A^2/c_s^2 [$c_s(r)$ and $c_A(r)$ being respectively the acoustic and Alfvén speeds due to the toroidal component of magnetic fields] is constant in the vertical direction, the radius where the vertical p-mode oscillations becomes purely vertical is determined by (Kato 2012b)

$$(\omega - m\Omega)^2 = \left(\frac{c_s^2 + c_A^2}{c_s^2 + c_A^2/2} K_{n,s} + 1 \right) \Omega_\perp^2, \quad (3)$$

where $K_{n,s}$ is a value resulting from the eigenvalue problem of the purely vertical oscillations and depending on the node number, n , in the vertical direction and the dimensionless height of truncation, z_s/H , H being the scale height of disks. The value of $K_{n,s} + 1$ is given in table 1 of Kato (2012c). $K_{n,s}$ is $n - 1$ in the limit of no truncation and larger than $n - 1$ in general cases.

As is shown above, the radii between the propagation and evanescent regions depends on the disk structure. Here, we write the boundary, for simplicity, in the form

$$(\omega - m\Omega)^2 = \psi \Omega_\perp^2 \quad (4)$$

and ψ is a parameter depending on disk structure. In the case of two-armed ($m = 2$) vertical p-mode oscillations, the boundary between the inner propagation and evanescent regions is thus given by

$$\omega = 2\Omega - \psi^{1/2} \Omega_\perp. \quad (5)$$

In general, ψ is larger than n [see equations (1) – (3)], and depends on n , c_A^2/c_s^2 , and z_s/H . In order to avoid complexity, we consider hereafter vertically isothermal disks with no truncation, i.e., $z_s = \infty$, and c_A^2/c_s^2 is assumed to be radially constant. Then, ψ is a function of b_T^2 for a given n as [see equation (3)]

$$\psi = \frac{1 + b_T^2}{1 + b_T^2/2} (n - 1) + 1, \quad (6)$$

where b_T^2 is a parameter defined by $b_T^2 \equiv c_A^2/c_s^2$. As is mentioned below, we are particularly interested in oscillations of $n = 2$ and $n = 3$. In the case of $b_T^2 = 0.4$, we have $\psi = 2.17$ for $n = 2$ and $\psi = 3.33$ for $n = 3$. Hence, in order to demonstrate typical examples of the frequency - radius relations given by equation (5) and (6), the relations in the case of $\psi = 2.17$ and $\psi = 3.33$ are shown in figures 1 and 2 by thin curves for different values of a_* . Figure 1 is for $a_* = 0.9$ and figure 2 is for $a_* = 0.5$. The mass of the central source is taken to be $10M_\odot$ in both figures. The left-hand side of the curves is the propagation region of the oscillations.

Next, let us consider the propagation region of axisymmetric g-mode oscillations. The region in the propagation diagram (frequency - radius diagram) is given by $\omega < \kappa$, when there is no poloidal magnetic fields in disks, and the boundaries of the propagation region of axisymmetric g-mode oscillation is specified by (Okazaki et al. 1987)

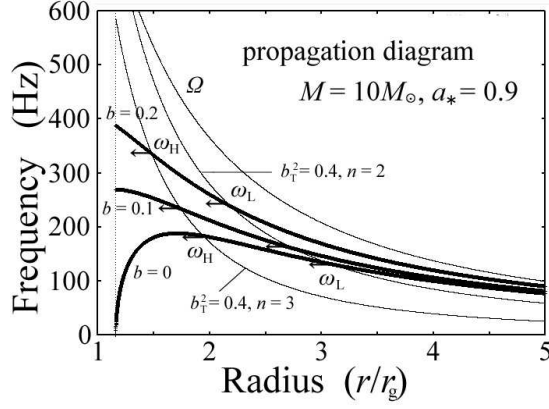


Fig. 1. Propagation diagram (frequency - radius relation) for axisymmetric ($m = 0$) g-mode oscillations and two-armed ($m = 2$) vertical p-mode oscillations in the case of $a_* = 0.9$ and $M = 10M_\odot$. Three thick curves give the relation of $\omega = \tilde{\kappa}$ for three cases of $b = 0, 0.1$, and 0.2 from bottom to top. The propagation regions of axisymmetric g-mode oscillation in disks with $b = 0, 0.1$, and 0.2 are, respectively, below the corresponding curve. Among three thin curves the lower two curves are $\omega = 2\Omega - (2.17)^{1/2}\Omega_\perp$ (i.e., $b_T^2 = 0.4$ and $n = 2$) and $\omega = 2\Omega - (3.33)^{1/2}\Omega_\perp$ (i.e., $b_T^2 = 0.4$ and $n = 3$). Two-armed vertical p-mode oscillations with $n = 2$ and $n = 3$ can propagate, respectively, below the corresponding curve in the case of $b_T^2 = 0.4$. The frequency given by the crossing point of two curves of $\omega = 2\Omega - (2.17)^{1/2}\Omega_\perp$ and $\omega = \tilde{\kappa}$ is the frequency of the lower HF QPOs, ω_L , in the present model. The waves with ω_L propagate inside the point in the diagram (shown by arrow). Similarly, the frequency given by the cross point of $\omega = 2\Omega - (3.33)^{1/2}\Omega_\perp$ and $\omega = \tilde{\kappa}$ is that of the upper HF QPOs. The waves with ω_H propagate inside the point in the diagram (shown by arrow).

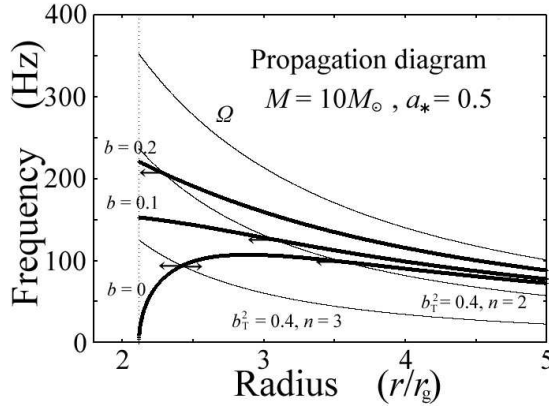


Fig. 2. The same as figure 1, except for $a_* = 0.5$. The curves of $\omega = 2\Omega - (2.17)^{1/2}\Omega_\perp$ (i.e., $b_T^2 = 0.4$ and $n = 2$) do cross with the curves of $\omega = \tilde{\kappa}$ in three cases of $b = 0, 0.1$, and 0.2 . The curve of $\omega = 2\Omega - (3.33)^{1/2}\Omega_\perp$ (i.e., $b_T^2 = 0.4$ and $n = 3$) crosses with the curve of $\omega = \tilde{\kappa}$ in the case of $b = 0$, but not in other cases of $b = 0.1$ and 0.2 . This shows the absence of ω_H and HF QPO will be single. It is noted that in the case of $b = 0$, ω_H is smaller than ω_L . Hence, in such cases the naming of ω_L and ω_H due to the order of frequency should be changed.

$$\omega = \kappa. \quad (7)$$

If poloidal magnetic fields exist, the radius specifying the boundary of propagation region of axisymmetric g-mode oscillations is strongly modified (Fu and Lai 2009). In the case of axisymmetric g-mode oscillations with $n = 1$, the propagation region is specified by $\omega < \tilde{\kappa}$ and $\tilde{\kappa}$ is given by (Fu and Lai 2009)

$$\tilde{\kappa}^2 = \frac{1}{2} \left[\kappa^2 + 2\Omega_{\perp}^2 b^2 + (\kappa^4 + 16\Omega_{\perp}^2 \Omega^2 b^2)^{1/2} \right], \quad (8)$$

where $b \equiv \tilde{c}_A/c_s$, \tilde{c}_A being the Alfvén speed defined by the poloidal component of magnetic fields. The frequency - radius relation given by

$$\omega = \tilde{\kappa} \quad (9)$$

is also shown in figures 1 and 2 by thick curves. Three cases of $b = 0, 0.1, \text{ and } 0.2$ are shown in each figure. The difference between figures 1 and 2 is the spin parameter, as mentioned before.

2.3. A Working Hypothesis Determining Frequency of Resonant Oscillations

The arguments given in subsection 2.2 are not enough to uniquely determine the frequency of resonantly excited oscillations, since the overlapping of the propagation regions is only a necessary condition. We should consider what case the growth of oscillations occur most strongly. To get a proper answer concerning this problem, detailed consideration on magnitude of coupling terms will be necessary. Instead, we are satisfied here with adopting a simple working hypothesis, as was done in the case of the warp resonant model (Kato 2004, 2008).

The excitation due to the resonance will be non-steady in the present problem in the sense that a wave will be excited at a place where the resonant interaction occurs most efficiently and then propagates in the radial direction. This wave will not satisfy in general the trapping condition. In other words, a possible condition determining the frequency of the excited oscillations will be that at the same radius the group velocities of both oscillations vanish together so that the resonant interaction occurs efficiently. In the limit of waves of short wavelength, the group velocity vanishes at the boundary between the propagation and evanescent regions [see, for example, an expression for group velocity given by equation (12.16) by Kato et al. (2008)]. The boundaries are nothing but the radii of Lindblad resonances in the case of p- and g- mode oscillations. In the above contexts, we impose, as the condition determining the frequency of resonant oscillation, that the boundary radius between the propagation and evanescent regions is the same for two resonantly interacting oscillations. As mentioned before, the boundary between the propagation and evanescent regions is given by equation (5) for the two-armed vertical p-mode oscillations, and by equation (9) for the axisymmetric g-mode oscillation. Thus, the crossing point of these two equations on the propagation diagram gives the frequency of the excited oscillations in the present model (see figures 1 and 2).

In the followings, the above-mentioned condition is examined in two cases of a highly spinning source ($a_* = 0.9$) and a less highly spinning source ($a_* = 0.5$). First, we consider the

coupling between a two-armed vertical p-mode oscillation with $n = 2$ and an axisymmetric g-mode oscillation with $n = 1$, taking $a_* = 0.9$ (figure 1).⁶ The mass of the central source is taken to be $10M_\odot$. If $\psi = 2.17$ (i.e., $b_T^2 = 0.4$ and $n = 2$) and $b = 0$ are adopted, the frequency is given by the crossing point of two curves of $\omega = 2\Omega - (2.17)^{1/2}\Omega_\perp$ and $\omega = \kappa$ on the propagation diagram (see figure 1), the point being one of those labelled by ω_L in figure 1. If $b = 0.1$ is adopted with other parameters unchanged, the point moves in the left-upper direction in the figure. If $b = 0.2$ is adopted, the point moves further in the left-upper direction. The point is also labelled by ω_L in figure 1. Similarly, we consider the interaction between the two-armed vertical p-mode oscillation with $n = 3$ and the axisymmetric oscillation with $n = 1$.⁷ Now, we take $\psi = 3.33$ (i.e., $b_T^2 = 0.4$ and $n = 3$). Then, the crossing point of two curves of $\omega = 2\Omega - (3.33)^{1/2}\Omega_\perp$ and $\omega = \tilde{\kappa}$ in three cases of $b = 0, 0.1$, and 0.2 is shown in figure 1. The points in two cases of $b = 0$ and 0.2 are shown by labelling ω_H . Here, we regards ω_L and ω_H in the same cases of parameters as the set of frequencies of the lower and upper HF QPOs.

Next, we consider the case of $a_* = 0.5$, keeping other parameters the same as those in corresponding cases of $a_* = 0.9$. As is shown in figure 2, we have no crossing point between the curve of $\omega = 2\Omega - (3.33)^{1/2}\Omega_\perp$ (i.e., $b_T^2 = 0.4$ and $n = 3$) and $\omega = \tilde{\kappa}$ in the region outside the radius of the marginally stable circular orbit, except for the case of $b = 0$. This comes from the following situations. Both curves of $\omega = 2\Omega - \psi^{1/2}\Omega_\perp$ and $\omega = \tilde{\kappa}$ shift downward on the propagation diagram as a_* decreases, but the former much moves downward compared with the latter. It is noted that in the case of no poloidal magnetic fields, the set of (ω_L, ω_H) always exist, but $\omega_L > \omega_H$. That is, for small a_* beyond at a certain value, the role of ω_L and ω_H is changed.

We should notice that in the present model, HF QPOs do not always appear in pairs as mentioned above. That is, in the sources with high spin or weak poloidal magnetic fields, they can appear in pairs, but in other cases, there is the possibility of only one or no HF QPOs.

3. Twin HF QPOs on Normalized Frequency – Frequency Diagram

In order to compare the set of ω_L and ω_H with observed frequencies of twin HF QPOs, we plot the set of $(\omega_L M, \omega_H M)$ on the $\omega_L M - \omega_H M$ diagram, where M is the mass of the central source. The reason why we consider the $\omega_L M - \omega_H M$ diagram is that the position of calculated $(\omega_L M, \omega_H M)$ on the diagram is independent of M , and depends only on the parameters a_* , b and b_T^2 .⁸ For various sets of (a_*, b_T^2) , the position of $(\omega_L M, \omega_H M)$ on the diagram is shown for three cases of $b = 0, 0.1$, and 0.2 (see subsequent subsections for individual source). Figure 3 is for $b = 0.1$, and figure 4 is for both $b = 0$ and $b = 0.2$. The value of a_* is changed continuously

⁶ These two oscillations can resonantly interact through the disk deformation, since the difference of n 's is 1 and is equal to one of n_D .

⁷ These two oscillations can resonantly interact since the difference of n 's is 2 and is equal to one of n_D .

⁸ If $z_s/H \neq \infty$, z_s/H is also an additional parameter.

from $a_* = 0.99$ towards $a_* = 0$, while b_T^2 is considered in four cases ($b_T^2 = 0, 0.2, 0.4$, and 0.6) in figure 3 and in three cases ($b_T^2 = 0, 0.2$, and 0.4) in figure 4. It is noted that the series of changing a_* with $b = 0.2$ are terminated at certain value of a_* (depending on b_T^2) before going to $a_* = 0$ (see the right-upper curves in figure 4). This is due to the absence of ω_H (and ω_L too in some cases) as mentioned before (compare figures 1 and 2).

Before evaluating (a_*, b, b_T^2) of four microquasars (GRS 1915+105, GRO J1655-40, XTE J1550-564, and H1743-322) by using the figures, we first draw a bird's eye view showing where twin HF QPOs of four microquasars are on this diagram. To do so, we adopt the following data for the microquasars:

$$\begin{aligned}
\text{GRS 1915 + 105} & : \omega_L^{\text{obs}} = 113\text{Hz}, \omega_H^{\text{obs}} = 168\text{Hz}, M = 10 - 18M_\odot \\
\text{GRO J1655 - 40} & : \omega_L^{\text{obs}} = 300\text{Hz}, \omega_H^{\text{obs}} = 450\text{Hz}, M = 5.1 - 5.7M_\odot \\
\text{XTE J1550 - 564} & : \omega_L^{\text{obs}} = 184\text{Hz}, \omega_H^{\text{obs}} = 276\text{Hz}, M = 8.5 - 9.5M_\odot \\
\text{H1743 - 322} & : \omega_L^{\text{obs}} = 166\text{Hz}, \omega_H^{\text{obs}} = 242\text{Hz}, M = 5.0 - 15.0M_\odot.
\end{aligned} \tag{10}$$

Observed lower and upper frequencies of the twin HF QPOs are denoted by ω_L^{obs} and ω_H^{obs} in order to distinguish them from the calculated ones. Here, the observed mass ranges of GRS 1915+105, GRO J1655-40, XTE J1550-564, and H1743-322 are taken, respectively, by referring to McClintock & Remillard (2006), Beer & Podsiadlowski (2002), Orosz et al. (2011), and Steiner et al. (2011), respectively.

Because of uncertainty of mass, the position of $(\omega_L^{\text{obs}}M, \omega_H^{\text{obs}}M)$ on the diagram is on a finite line with a gradient of roughly 3:2 for each source. Since the ranges of the lines for four sources overlap on the diagram, we present the ranges by introducing rectangles whose diagonal shows the range. Using this convention, we overdraw in figures 3 and 4 the ranges of position of $(\omega_L^{\text{obs}}M, \omega_H^{\text{obs}}M)$ of the observed HF QPOs of the four microquasars by rectangles.

It is noted that the position of twin QPOs by the epicyclic resonant model (Ep) (Kluźniak & Abramowicz 2001) and the warp resonant model (Wp) (Kato 2008) are also shown, for reference, in figure 3 for some values of a_* . These models have no other parameter than a_* . Hence, the position of twin HF QPOs by these models is determined only by a_* .

In figure 3 (and figure 4) the most probable points of $(\omega_L^{\text{obs}}M, \omega_H^{\text{obs}}M)$ of the four microquasars on the $(\omega_L M, \omega_H M)$ diagram are all roughly around the center of the figure. This suggests that the four microquasars belong all to a similar class. Furthermore, comparison of figure 3 with figure 4 shows that $b = 0.1$ is better than $b = 0$ and $b = 0.2$ to describe observations. That is, figure 4 shows that if $b = 0$, the present model cannot describe observations even if a_* is taken as high as $a_* \sim 1$, unless each mass of microquasars is taken to be smaller than each mean value in the observationally allowed range given in equation (10). Figure 4 further shows that $b = 0.2$ is too large to describe observations in the same sense mentioned above. In other words, if the present model is correct, the poloidal magnetic fields in disks in these four microquasars will roughly be around $b \simeq 0.1$.

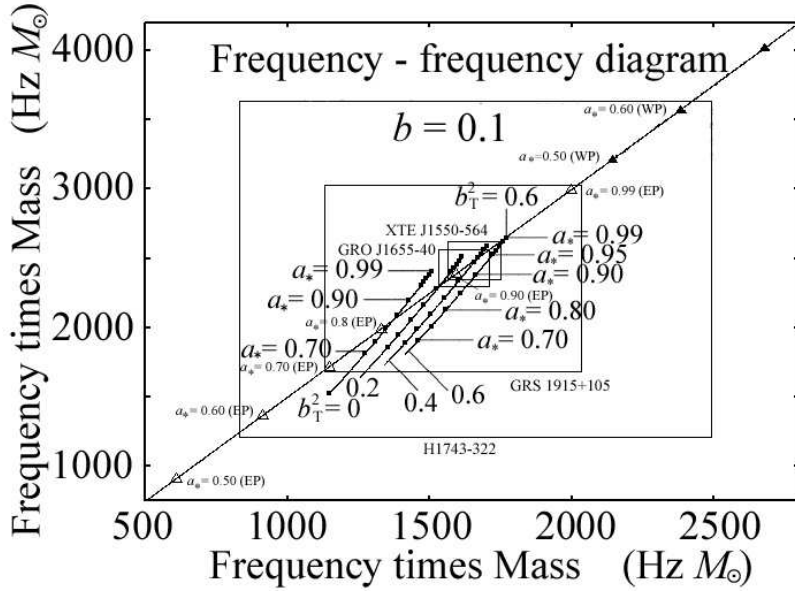


Fig. 3. Relation between $\omega_L M$ and $\omega_H M$ on frequency - frequency diagram normalized by mass of the central source, i.e., the coordinates are frequency times mass. The relation is specified by three parameters, which are a_* , b , and b_T^2 . The latter two are related to magnetic structure of disks, i.e., b is to the strength of poloidal magnetic fields and b_T^2 to that of toroidal magnetic fields. In this figure b is taken to be $b = 0.1$. Four curves are for $b_T^2 = 0.0, 0.2, 0.4,$ and 0.6 (from left to right), a_* being changed from 0.99 to lower values. The upper end of each curve is for $a_* = 0.99$. Positions of four microquasars (GRS 1915+105, GRO J1655-40, XTE J1550-564, H1743-322) on the diagram are shown by rectangles. That is, due to uncertainties of mass, the position of $(\omega_L M, \omega_H M)$ of each source on the diagram is on the line of diagonal of each rectangle specified by each source. For reference, the position of frequency - frequency relation by epicyclic model (Ep) and warp model (Wp) are also shown by open angles and filled angles, respectively. The straight line running from left-bottom to right-top is the line on which the frequency ratio is 3 : 2.

Restricting only to the case of $b = 0.1$, we estimate the values of other parameters, especially the spin parameter a_* in order to examine whether it is consistent with that estimated from spectral analyses. Hereafter, we discuss the four microquasars separately.

3.1. GRS 1915+105

Figure 5 is an extension of a part of figure 3. The diagonal of the large rectangle covering the almost all area of figure 5 shows the range of the possible position of the set of observed twin QPOs, when the mass range is taken to be $M = 10 - 18M_\odot$. The small filled rectangles on the diagonal in figure 5 is the position of the twin QPOs in the cases where the mass is taken from $10M_\odot$ to $18M_\odot$. The four lines running in the middle region of the figure are for $b_T^2 = 0.0, 0.2, 0.4,$ and 0.6 from left to right, changing the value of a_* . On each line the upper end point is for $a_* = 0.99$. This figure shows that the set of (a_*, b_T^2) which can describe the observed set of QPO frequencies are $(\sim 0.93, \sim 0.3)$ if $M = 14M_\odot$, and $(0.99, \sim 0.7)$ if $M = 16M_\odot$.

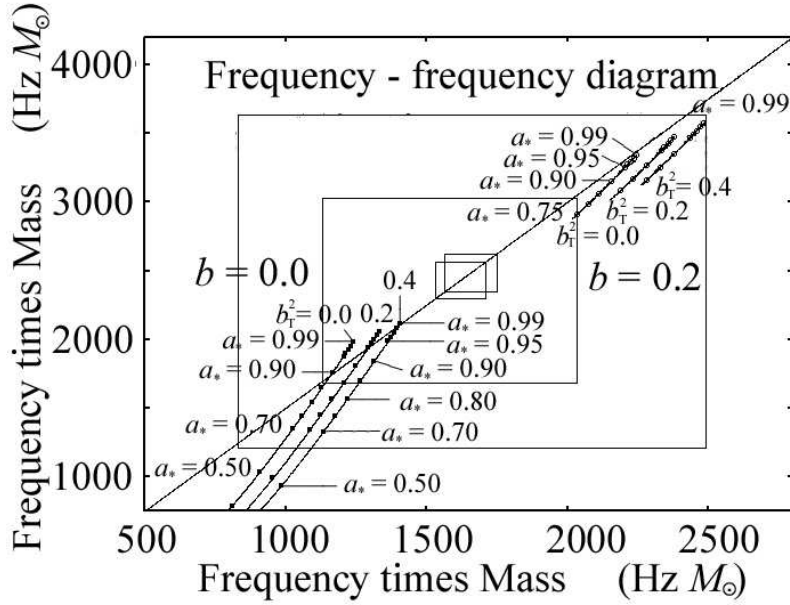


Fig. 4. The same as figure 3 except that in this figure the frequency - frequency relation in two cases of $b = 0$ and $b = 0.2$ are shown.

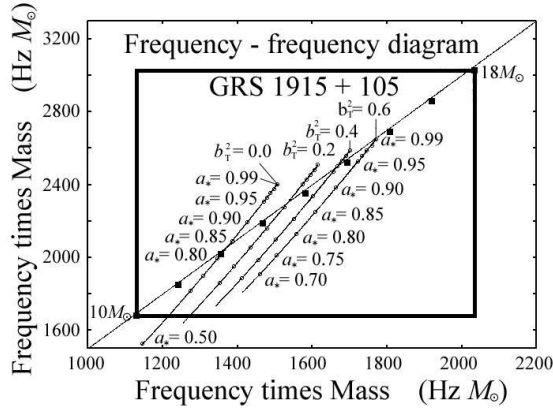


Fig. 5. An extension of figure 3 so that we can inspect what set of (a_*, b_T^2) will describe the observed twin HF QPOs of GRS 1915+105 in the case where $b = 0.1$ is adopted.

If $M > 16M_\odot$, the present model cannot describe the observed twin QPOs as long as $b = 0.1$ is adopted, since the value of a_* required becomes larger than unity. In other words, if this source has really $M > 16M_\odot$ and the present model is correct, the poloidal magnetic fields of this source are slightly stronger than $b = 0.1$. It is noticed that if b is larger than $b = 0.1$, the curves on figure 5 shift in the right-upward direction, and observations can be described by a_* smaller than unity (compare figures 3 and 4). A large value of a_* presented here is consistent with $a_* > 0.98$ derived from spectral analyses (McClintock & Remillard 2006).

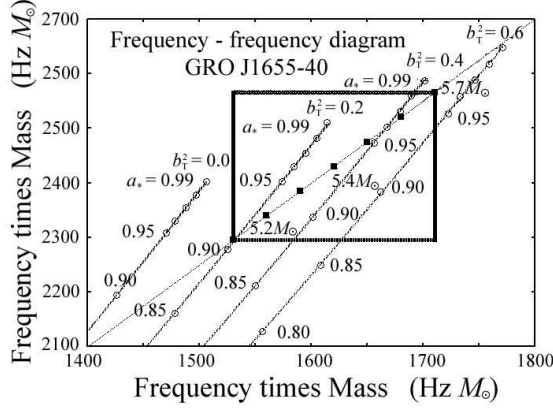


Fig. 6. An extension of figure 3 so that we can inspect what set of (a_*, b_T^2) will describe the observed twin HF QPOs of GRO J1655-40 in the case where $b = 0.1$ is adopted.

3.2. GRO J1655-40

Figure 6 is for GRO J1655-40, and the same as figure 5 except that the twin QPO frequencies are taken here to be $\omega_L^{\text{obs}} = 300\text{Hz}$ and $\omega_H^{\text{obs}} = 450\text{Hz}$. Figure 6 shows that the set of (a_*, b_T^2) which can describe observations are $(\sim 0.90, 0.2)$ when $M = 5.1M_\odot$, and $(\sim 0.95, \sim 0.4)$ when $M = 5.5M_\odot$, and $(\sim 0.99, \sim 0.5)$ when $M = 5.7M_\odot$. The spin estimated from spectral analyses is $a_* = 0.70 - 0.80$ (Shafee et al. 2006) and $a_* \sim 0.98$ (Miller et al. 2011). Our results are closer to the latter, as long as $b = 0.1$ is adopted. If b is slightly larger than $b = 0.1$, however, a smaller a_* (with a smaller b_T^2) fits observations (compare figures 3 and 4).

3.3. XTE J1550-564

Figure 7 is for XTE J1550-564, since $\omega_L^{\text{obs}} = 184\text{Hz}$ and $\omega_H^{\text{obs}} = 276\text{Hz}$ are adopted. This figure shows that the set of (a_*, b_T^2) which can describe observed twin QPO frequencies are $(\sim 0.92, \sim 0.2)$ when $M = 8.5M_\odot$, and $(\sim 0.96, 0.4)$ for $M = 9.1M_\odot$. The value of spin parameter a_* required by the present model is rather high compared with the value derived from spectral analyses. The latter is $a_* \sim 0.5$ in average (Steiner et al. 2011) or $a_* = 0.70 - 0.75$ (Miller et al. 2009).

This difference will be accounted for if this source has a stronger poloidal magnetic fields than GRS 1915+105 in the sense that $b > 0.1$. This is because if $b > 0.1$, the calculated curves in figure 7 shift in the upper-right direction in the figure, as mentioned before in relation to GRO J1655-40 (compare figures 3 and 4).

3.4. H1743-322

Figure 8 is for H1743, since this diagram is drawn by taking $\omega_L^{\text{obs}} = 166\text{Hz}$ and $\omega_H^{\text{obs}} = 242\text{Hz}$. This figure shows that the set of (a_*, b_T^2) which can describe observations are $(\sim 0.80, \sim 0)$ for $M = 8M_\odot$, $(\sim 0.9, \sim 0.2)$ for $M = 9M_\odot$, and $(0.93, 0.4)$ for $M = 10M_\odot$. The present model

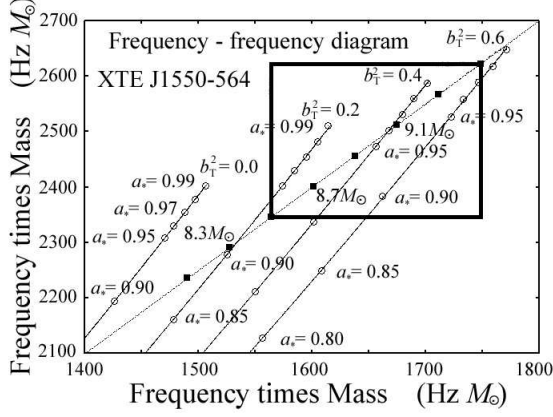


Fig. 7. An extension of figure 3 so that we can inspect what set of (a_*, b_T^2) will describe the observed twin HF QPOs of XTE J1550-564 in the case where $b = 0.1$ is adopted.

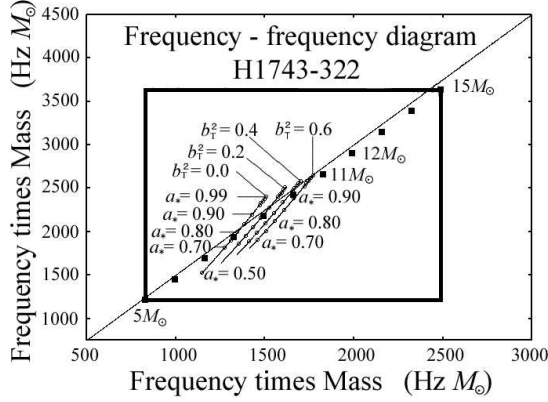


Fig. 8. An extension of figure 3 so that we can inspect what set of (a_*, b_T^2) will describe the observed twin HF QPOs of H1743-322 in the case where $b = 0.1$ is adopted.

cannot describe observations if $M > 11M_\odot$, as long as $b = 0.1$ is adopted. Steiner et al. (2011) estimate a_* to be smaller than 0.7 by spectral analyses. This difference of our a_* and that of Steiner et al. (2011) can be accounted for if stronger poloidal magnetic fields than $b = 0.1$ are present in H1743, as in the case of XTE J1550-564.

4. Discussion

A standpoint of this model is that the 3 : 2 frequency ratio observed in twin HF QPOs of microquasars does not come from their excitation processes, but occurs by chance. In the present model, a quasi-periodic oscillation is a result of a resonant interaction between two oscillations with positive and negative energies through disk deformation (Kato et al. 2011). As the disk deformation, a two-armed ($m_D = 2$) deformation is assumed, different from our

previous studies where an one-armed ($m_D = 1$) deformation is considered (e.g., Kato 2004, 2008). As the set of positive and negative energy waves, we consider an axisymmetric ($m = 0$) g-mode oscillation with positive energy and a two-armed ($m = 2$) vertical p-mode oscillation with negative energy.

The difference of azimuthal wavenumber in the above two disk oscillations is two, which is equal to the azimuthal wavenumber, m_D , of the disk deformation. Hence, a necessary resonant condition among azimuthal wavenumbers of the two oscillations and the disk deformation is satisfied. For the resonance really to occur, a relation among vertical node number is also necessary for the two oscillations and the disk deformation. In this paper we have considered *two* two-armed vertical p-mode oscillations with two nodes ($n = 2$) and three nodes ($n = 3$). On the other hand, as an axisymmetric g-mode oscillation, we have considered the mode with one node ($n = 1$) in the vertical direction. Hence, for these vertical p-mode oscillations to resonantly interact with the g-mode oscillations through the disk deformation, the disk deformation must have both components of $n = 1$ and $n = 2$. The deformation with $n = 1$ is the fundamental deformation of disks which is anti-symmetric with respect to the equator.

One of vague points of this model is how much the assumption concerning the frequency of excited oscillations (i.e., coincidence of boundaries of propagation regions for two interacting oscillations) is relevant or not. To study this problem in details, we must examine functional forms in the radial and vertical directions of two interacting positive and negative energy oscillations and evaluate the volume integration of coupling terms by using those functional forms of oscillations and disk deformation [see Kato (2008) as an example of detailed calculations of the coupling terms]. This is a complicated problem and beyond the scope of this paper.

Different from the kHz QPOs in neutron-star LMXBs, the observed frequencies of twin QPOs of black-hole LMBXs are robust, they being time-independent and their ratio being close to 3 : 2. Furthermore, for four microquasars considered in this paper, the observational points of $(\omega_H^{\text{obs}}M, \omega_L^{\text{obs}}M)$ on the $(\omega_H M, \omega_L M)$ diagram are close when the typical observational values of M 's are adopted for each source (see that the centers of four rectangles in figure 1 are close). These observational evidences suggest that the disks of these sources are roughly in a similar state with similar time-independent values of disk parameters. In the present model we have two dimensionless disk parameters describing the magnetic structure of the innermost region of disks. They are b and b_T , where $b \equiv \tilde{c}_A/c_s$ and $b_T \equiv c_A/c_s$, \tilde{c}_A and c_A being the Alfvén speed defined by the poloidal and toroidal magnetic fields in disks, respectively, and c_s being the acoustic speed. As discussed in the text, $b \geq 0.1$ and $b_T = (0.2)^{1/2} \sim (0.4)^{1/2} = 0.45 \sim 0.63$ seem to be relevant to describe observations. Detailed comparison of the present model with observations will not be instructive at the present stage, since the validity of the working hypothesis mentioned in subsection 2.3 might not be clear enough. The strength of magnetic fields required to describe the QPO frequencies of the four microquasars by the present model is, however, in a narrow range as noticed above. This may suggest that the strength of magnetic

fields in disks is self-adjusted by a balance between winding by differential rotation and release by jet ejection.

In the present model, QPOs are not always in pairs. In some sources there is only one QPO or no QPO, depending on parameters. For example, in disks with $b = 0.2$ and $b_{\text{T}}^2 = 0.4$, two QPOs ($n = 2$ and $n = 3$) are present when $a_* = 0.9$ (see figure 1), but QPO is only one ($n = 2$) if a_* is as small as 0.5 (see figure 2), because the curve of $\omega = 2\Omega - \psi^{1/2}\Omega_{\perp}$ for $n = 3$ (with $b_{\text{T}}^2 = 0.4$) is below the curve of $\omega = \tilde{\kappa}$ (with $b = 0.2$) in all radius. Even the QPO of $n = 2$ disappears (there is no QPO) if b_{T}^2 is slightly larger than $b_{\text{T}}^2 = 0.4$ ($b = 0.2$ and $a_* = 0.5$), as understand from figure 2. Next, let us consider sources with $b = 0$. In this case, there are always two QPOs as shown in figures 1 and 2. However, in the case of figure 2 ($a_* = 0.5$), the cross point between $\omega = \kappa$ and $\omega = 2\Omega - \psi^{1/2}\Omega_{\perp}$ occurs inside the radius where κ becomes the maximum, as is shown in figure 2. In this case the propagation regions of the two oscillations are in the oposite side of the crossing point, and there is no overlapping region of the two oscillations. In such cases, the coupling of the two oscillations and thus excitation of the oscillations will be weak. In summary, we can say that the sources where twin QPOs are observed are those where the disk parameters are in some limited range with strong spin parameter. This might be one of reasons why twin QPOs are observed only in limited sources.

Finally, we should note that we have an important disk parameter which was not considered in this paper, but will affect results. This is the vertical thickness of disks, z_s . In this paper we assumed that the disk is isothermal in the vertical direction and extends infinitely. In actual situations, the disks will be truncated in the vertical thickness at a certain height, z_s , by the presence of corona. In such disks, the propagation region of the two-armed vertical p-mode oscillations is modified (Kato 2012b,c), which changes ω_{H} and ω_{L} . This will be a problem to be examined. It is noticed that retreat of the inner edge of disks from the radius of the marginally stable circular orbit has no serious effects on results of the present model, since the oscillations treated in the model are not standing ones and no inner boundary condition is imposed to the oscillations.

A note added on July 24, 2012.

In order to examine validity of the wave excitation mechanism adopted in this paper [i.e., excitation of a set of waves with positive and negative wave energies through a resonant coupling with disk deformation (Kato et al. 2011)], we consider waves in tidally deformed disks of binary stars. It is found that the tidal instability and superhump phenomena in dwarf novae can well be interpreted by the mechanism. This will be shown in a subsequent paper.

References

- Abramowicz, M.A. & Kluźniak, W. 2001, *A&A*, 374, L19
 Abramowicz, M.A., Bulik, T., Bursa, M., & Kluźniak, W. 2003a, *A&A*, 404, L21
 Abramowicz, M.A., Karas, V., Kluźniak, W., Lee, W.H., & Rebusco, P. 2003b, *PASJ*, 55, 466

- Beer, M.E., & Podsiadlowski, P. 2002, MNRAS, 331, 351
- Bursa, M., Abramowicz, M.A., Karas, V.W., & Kluźniak, W. 2004, ApJ, 617, L45
- Greene, J., Bailyn, C.D., & Orosz, J.A. 2001, ApJ, 554, 1290
- Ferreira, B.T., & Ogilvie, G.I. 2008, MNRAS, 386, 2297
- Fu, W. & Lai, D., 2009, ApJ, 690, 1386
- Harlaftis, E.T. & Greiner, J. 2004, A&A, 414, 13
- Horák, J. 2008, A&A, 486, 1
- Horák, J., Abramowicz, M.A., Kluźniak, W., Rebusco, P., & Torok, G. 2009, A&A, 499, 540
- Kato, S. 2001, PASJ, 53, 1
- Kato, S. 2003, PASJ, 55, 801
- Kato, S. 2004, PASJ, 56, 905
- Kato, S. 2005, PASJ, 57, 699
- Kato, S. 2008, PASJ, 60, 111
- Kato, S. 2010, PASJ, 62, 635
- Kato, S. 2011a, PASJ, 63, 125 (toriodal mag. fields)
- Kato, S. 2011b, PASJ, 63, 617 (double diffusion)
- Kato, S. 2011c, PASJ, 63, 861 (toroidal, kHz QPOs)
- Kato, S. 2012a, PASJ, 64, in press
- Kato, S. 2012b, PASJ, 64, in press
- Kato, S. 2012c, PASJ, submitted
- Kato, S. & Fukue, J. 1980, PASJ, 32, 377
- Kato, S. & Fukue, J. 2006, PASJ, 58, 909
- Kato, S., Fukue, J., & Mineshige, S. 2008, Black-Hole Accretion Disks — Towards a New paradigm — (Kyoto: Kyoto University Press), chaps. 3 and 11
- Kato, S., Okazaki, A.T., & Ohtariani, F. 2011, 63, 363
- Kluźniak, W. & Abramowicz, M.A. 2001, Acta Phys. Pol.B32, 3605
- Kluźniak, W., Abramowicz, M.A., Kato, S., Lee, W.H., & Stergioulas, N. 2004, ApJ, 603, 89
- Machida, M., & Matsumoto, R. 2008, PASJ 60, 613
- McClintock, J.E., Remillard, R. 2006, ARA&A, 44, 49
- McClintock, J.E., Shafee, R., Narayan, R., Remillard, R.A., Davis, S.W., & Li, L. 2006, ApJ, 652, 518
- McClintock, J.E., Narayan, R., Davis, S.W., Gou, L., Kulkarni, A., Orosz, J.A., Penna, R.F., Remillard, R., & Steiner, J.F., 2011, Classical and Quantum Gravity, special volume for GR19, eds., D.Maraff, D. Sudarsky
- Miller, J.M., Reynolds, C.S., Fabian, A.C., Miniutti, G., & Gallo, L.C. 2009, ApJ, 697,900
- Morsink, S.M. & Stella, L. 1999, ApJ, 513, 827
- Okazaki, A.T., Kato, S., & Fukue, J. 1987, PASJ, 39, 457
- Ohtariani, f., Okazaki, A.T., & Kato, S. 2010, 62, 709

- Orosz, J.A. et al. ApJ, 568, 8450
- Penninx, W. 1989, in J.Hunt, & B.Battrick, eds. "Proceedings of the 23rd ESLAB symposium on Two Topics in X-ray Astronomy", Bologna, Sept. 1989, ESA publications ESA SP-296, 185
- Perez, C.A., Silbergleit, A.S., Wagoner, R.V., & Lehr, D.E. 1997, ApJ, 476, 589
- Priedhorsky, W., Hasinger, G., & Lawin, W.H.G., et al. 1986, ApJ, 306,L91
- Rebusco, P. 2004, PASJ, 56,553
- Remillard, R. 2005, Astron. Nachr. 326, 804
- Shafee, R., McClintock, J.E., Narayan, R., Davis, S.W., Li, L.,& Remillard, R.A. 2006, APJ, 636, L113
- Silbergleit, A.S., Wagoner, R.V., & Ortega-Dodríguez, M. 2001, ApJ., 548, 335
- Steiner, J.F., Reis, R.C., McClintock, J.E., Narayan, R., Remillard, R.A., Orosz, J.A., Gou, L., Fabian, A.C., & Torres, M.A.P. 2002, MNRAS, 416, 941
- Stella, L., & Vietri, M. 1998, ApJL, 492, L59
- Stuchlik, Z., Konar, S., Miller, J.C., & Hledik, S. 2008a, A&A, 489, 963
- Stuchlik, Z., Kotrlova, A., & Torok, G. AcA, 58, 441
- Török, G. 2011, A&A, 531, 59
- Török, G., Kotrlova, A., Sramkova, E., & Stuchlik, Z. 2011, A&A, 531, 59
- van der Klis, M. 2004, in Compact stellar X-ray sources (Cambridge University Press), eds. W.H.G. Lewin and M. van der Klis (astro-ph/0410551)
- Wagoner, R.V. 1999, Phys. Rep. 311, 259
- Wagoner, R.V. 2011, ApJL, in press (ArXiv:1205.1783)